Virtual and In Vitro Screens Reveal a Potential Pharmacophore that Avoids the Fibrillization of Aβ$_{1-42}$

Maricarmen Hernández-Rodríguez[1,2], José Correa-Basurto[1]*, María Inés Nicolás-Vázquez[3], René Miranda-Ruvalcaba[3], Claudia Guadalupe Benítez-Cardoza[4], Aldo Arturo Reséndiz-Albor[5], Juan Vicente Méndez-Méndez[6], Martha C. Rosales-Hernández[2]*

1 Laboratorio de Modelado Molecular y Diseño de Fármacos, Escuela Superior de Medicina, Instituto Politécnico Nacional, Plan de San Luis y Díaz Mirón S/N, Delegación Miguel Hidalgo, México D.F., México, 2 Laboratorio de Biofísica y Biocatálisis, Escuela Superior de Medicina, Instituto Politécnico Nacional, Plan de San Luis y Díaz Mirón S/N, Delegación Miguel Hidalgo, México D.F., México, 3 Quimica inorgánica-orgánica del Departamento de Ciencias Químicas, de la Facultad de Estudios Superiores Cuautitlán Campo 1, Universidad Nacional Autónoma de México, Avenida 1o de Mayo S/N, Santa María las Torres, Cuautitlán Izcalli, Estado de México, México, 4 Laboratorio de Investigación Bioquímica, Sección de Estudios de Posgrado e Investigación, Escuela Nacional de Medicina y Homeopatía, Instituto Politécnico Nacional, Guillermo Massieu H 239, Gustavo A. Madero, La Escalera, México D.F., México, 5 Laboratorio de Investigación en Inmunología., Escuela Superior de Medicina, Instituto Politécnico Nacional, Plan de San Luis y Díaz Mirón S/N, Delegación Miguel Hidalgo, México D.F., México, 6 Centro de Nanociencias y Micro y Nanotecnología, Instituto Politécnico Nacional, Luis Enrique Erro S/N, U. Prof Adolfo López Mateos, Gustavo A. Madero, México D.F., México

* marcrh2002@yahoo.com.mx (MCRH); corrjose@gmail.com (JCB)

Abstract

Among the multiple factors that induce Alzheimer's disease, aggregation of the amyloid β peptide (Aβ) is considered the most important due to the ability of the 42-amino acid Aβ peptides (Aβ$_{1-42}$) to form oligomers and fibrils, which constitute Aβ pathological aggregates. For this reason, the development of inhibitors of Aβ$_{1-42}$ pathological aggregation represents a field of research interest. Several Aβ$_{1-42}$ fibrillization inhibitors possess tertiary amine and aromatic moieties. In the present study, we selected 26 compounds containing tertiary amine and aromatic moieties with or without substituents and performed theoretical studies that allowed us to select four compounds according to their free energy values for Aβ$_{1-42}$ in α-helix (Aβ-α), random coil (Aβ-RC) and β-sheet (Aβ-β) conformations. Docking studies revealed that compound 5 had a higher affinity for Aβ-α and Aβ-RC than the other compounds. *In vitro*, this compound was able to abolish Thioflavin T fluorescence and favored an RC conformation of Aβ$_{1-42}$ in circular dichroism studies, resulting in the formation of amorphous aggregates as shown by atomic force microscopy. The results obtained from quantum studies allowed us to identify a possible pharmacophore that can be used to design Aβ$_{1-42}$ aggregation inhibitors. In conclusion, compounds with higher affinity for Aβ-α and Aβ-RC prevented the formation of oligomeric species.

Introduction

Alzheimer's disease (AD) is a progressive neurodegenerative disorder that is characterized by extracellular fibrillary deposits and intracellular neurofibrillary tangles [1]. The primary component of the AD-associated extracellular deposits is a 4-kD peptide that is commonly known as amyloid-β (Aβ) [2]. Aβ originates from the Aβ precursor protein [3], which is hydrolyzed by the β- and γ-secretases to release Aβ peptides containing 39–43 amino acid residues. However, the most important peptide contains 42 residues ($A\beta_{1-42}$) [4]. During fibrillogenesis, $A\beta_{1-42}$ undergoes a conformational change from an α-helix to parallel β-sheets, which are connected by a bent structure encompassing residues 23–29, and the close distance between the side chains of Asp23 and Lys28 forms an electrostatic interaction [5]. This curved structure may be rate-limiting in fibril formation [6]. In recent years, the formation of amyloid fibrils has been shown to be more complex than a linear sequential monomer-to-fibril reaction and consists of several toxic intermediates, including soluble oligomers [7–8], that can bind to hippocampal neurons and induce synaptic plasticity dysfunction [9].

Therefore, many Aβ fibrillogenesis inhibitors that contain aromatic rings and/or amines have been identified through compound library screens and by rational design strategies [10–12]. However, these compounds bind to the elongated β-sheet conformation of $A\beta_{1-42}$ to prevent its polymerization [12–16]. A potential problem with this strategy is that blocking the later stages of fibril formation favors the formation of the prefibrillary oligomeric forms that are even more cytotoxic than the fibrils [10]. Furthermore, the evaluation of pharmacophores that prevent amyloid aggregation has been proposed, but these pharmacophores have only been evaluated during the fibrillization process and, in some cases, only target a segment of $A\beta_{1-42}$ [17–18]. Thus, the design of compounds with greater affinity for the α-helix or random coil (RC) conformations of $A\beta_{1-42}$ than the β-sheet conformation could block the adoption or destabilization of the $A\beta_{1-42}$ β-sheet and could be good oligomerization inhibitors [19–21].

Using *in silico* and *in vitro* studies, our group has demonstrated that electrostatic interactions between the lateral chains of Glu22 and Asp23 in the $A\beta_{1-42}$ turn conformation and a chemical group with a positive charge (such as copper) prevent the formation of the turn, which is necessary during the pathological aggregation of $A\beta_{1-42}$ [22]. In addition, molecular dynamics (MD) simulations have demonstrated that the π–π interaction between the lateral chains of Phe19 and Phe20 favors the α-helix to β-sheet conformational change [21].

In the present study, we focused on small ligands that have tertiary amine and aromatic moieties with or without substituents to identify a possible pharmacophore that could prevent the salt bridge formation and consequently avoid the adoption of the β-sheet conformation of $A\beta_{1-42}$. Twenty-six ligands were chosen from the Sigma–Aldrich database and subjected to docking studies to evaluate their binding affinity and free energy values (ΔG) on three different conformations of $A\beta_{1-42}$ (α-helix, random coil and β-sheet). Based on their affinity toward the $A\beta_{1-42}$ conformations, we selected four compounds (compounds 5, 8, 14 and 19) and used the Thioflavin T (ThT) fluorescence assay to evaluate their *in vitro* activities as $A\beta_{1-42}$ fibrillization inhibitors. The conformation of $A\beta_{1-42}$ in the presence of these compounds was evaluated using circular dichroism (CD) spectroscopy, and the morphology of $A\beta_{1-42}$ was determined using atomic force microscopy (AFM). Once the *in vitro* activity was evaluated, the IC_{50} values of compounds 5 and 8 were determined. Finally, quantum chemistry studies were performed to analyze the electronic behavior and the molecular basis of $A\beta_{1-42}$ recognition by compounds 5 and 8.

Materials and Methods

Because most of the ligands that can inhibit $A\beta_{1-42}$ oligomerization possess an amine and an aromatic ring [10–12], 26 ligands (Fig 1) with a molecular weight (MW) of <500 and with amine and aromatic moieties were chosen for docking studies to evaluate their binding to $A\beta_{1-42}$. Among these compounds, we selected acetylcholine (ACh) to evaluate the influence of the lack of an aromatic group in the recognition by $A\beta_{1-42}$ (Fig 1; compound 26). The MarvinSketch server (http://www.chemaxon.com/marvin/sketch/index.jsp) was used to determine the protonation state (pKa) of the compounds according to the ionizable groups at physiological pH (7.35–7.45).

Ligand selection

Because most of the ligands that can inhibit $A\beta_{1-42}$ oligomerization possess an amine and an aromatic ring [10–12], 26 ligands (Fig 1) with a molecular weight (MW) of <500 and with amine and aromatic moieties were chosen for docking studies to evaluate their binding to $A\beta_{1-42}$. Among these compounds, we selected acetylcholine (ACh) to evaluate the influence of the lack of an aromatic group in the recognition by $A\beta_{1-42}$ (Fig 1; compound 26). The MarvinSketch server (http://www.chemaxon.com/marvin/sketch/index.jsp) was used to determine the protonation state (pKa) of the compounds according to the ionizable groups at physiological pH (7.35–7.45).

Molecular docking

We selected three $A\beta_{1-42}$ structures in different structural conformations to sample different $A\beta_{1-42}$ conformations. Two of them were obtained from the Protein Data Bank (www.rcsb.org). The first corresponds to $A\beta_{1-42}$ in an α-helix, PDB id: 1Z0Q, and the second corresponds to $A\beta_{17-42}$ in a β-sheet, PDB id: 2BEG. Both structures have been employed in several research studies [22–25]. The structure of the RC conformation corresponds to the $A\beta_{1-42}$ conformer obtained at 10 ns through molecular dynamics (MD) simulations of 1ZOQ, which has been reported by our research group [26]. Additionally, the percentages of secondary structures for each Aβ conformation were calculated using the stride server [27] to provide information on the $A\beta_{1-42}$ structures employed.

To prepare the structures for docking studies, all of the possible rotable bonds and partial atomic charges (Gasteiger-Marsili formalism) of the ligands, as well as the Kollman charges for all of the atoms in the peptide, were assigned using AutoDock Tools version 3.4 [28]. The ligands were docked on the $A\beta_{1-42}$ conformers using AutoDock version 4.2.0 with the hybrid Lamarckian Genetic Algorithm as the search method, an initial population of 100 randomly placed individuals and a maximum of 1.0×10^7 energy evaluations [29]. The resulting docked orientations that were clustered together occurred within a root mean square deviation of 0.5 Å. The lowest free energy cluster for each docked orientation returned by AutoDock was used for further analysis, and all other parameters were maintained at the default settings [29]. The docking procedure was centered on Glu22 and Asp23, using a grid box $60 \times 60 \times 60$ Å, with the grid points separated by 0.375 Å. All protein visualizations were performed with PyMol viewer [30]. The lowest energy cluster for each ligand was subjected to further free energy (ΔG) and binding geometry analyses, as previously reported [28].

Evaluation of $A\beta_{1-42}$ aggregation by ThT fluorescence

Once the docking studies yielded results that allowed us to select four compounds for experimental studies, we evaluated their effect on $A\beta_{1-42}$ pathological aggregation. For this purpose,
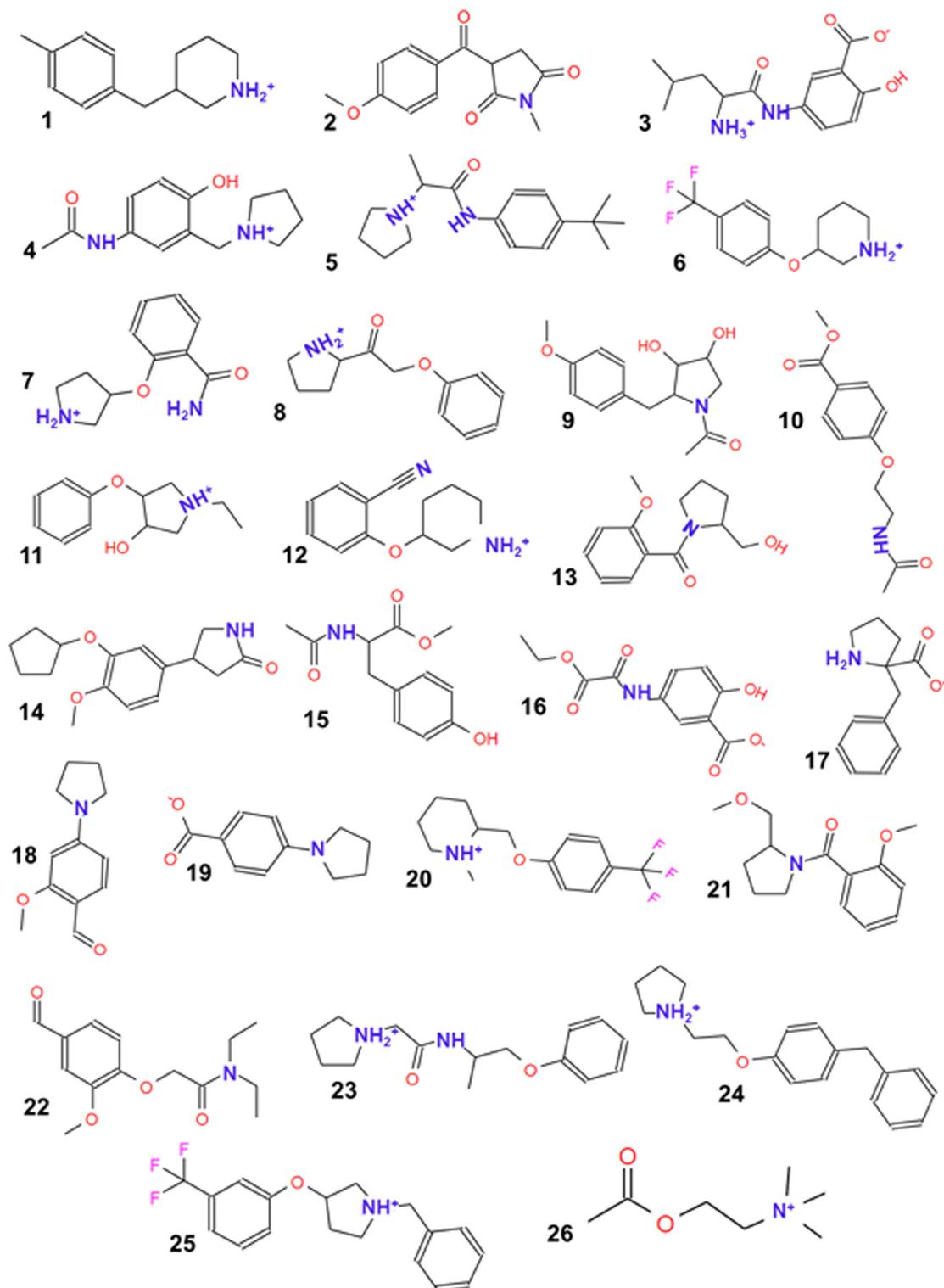
Fig 1. Chemical structures of the selected compounds used as possible Aβ$_{1-42}$ oligomerization inhibitors. All of the compounds selected contained an amine and/or aromatic ring in their structure. However, not all of the compounds could acquire a positive charge at physiological pH. The compounds are shown with their protonation states based on their pKas.

lyophilized wild-type human Aβ$_{1-42}$ peptide (chloride salt) was purchased from Calbiochem (Mexico). HEPES sodium salt (>99.5% purity) and ThT were obtained from Sigma–Aldrich (Mexico). A freshly prepared Aβ$_{1-42}$ solution (50 μM in fresh MilliQ water) was incubated alone and in the presence of the selected compounds (100 μM) [26]. The samples were incubated at 37°C in a 0.5-cm path length quartz cell and stirred at 250 rpm. The increase in ThT fluorescence [31] was measured using a Perkin–Elmer LS-55 fluorescence spectrophotometer equipped with a water-jacketed cell holder for temperature control. The emission and excitation wavelengths were 445 and 480 nm, respectively. The fluorescence emission recordings were made using path-length quartz cuvettes. The buffer solution was 20 mM HEPES and 100 mM NaCl, pH 7.4, containing 3.3 μM ThT [26]. The inhibition of Aβ$_{1-42}$ pathological aggregation for compounds 5, 8, 14 and 19 was calculated after 24 h of incubation.

CD measurements

The lyophilized wild-type human Aβ$_{1-42}$ peptide was diluted in MilliQ water to a final concentration of 50 μM, as reported previously [11]. The Aβ$_{1-42}$ solution was incubated at 37°C in the absence and presence of the target compounds. CD spectra were acquired using a JASCO J-815 spectropolarimeter (Jasco, Easton, MD, USA) equipped with a PFD-425S Peltier-type cell holder for temperature control at 37°C and magnetic stirring. The CD spectra were recorded from 180 to 250 nm using 1.0-mm path-length quartz cells. The data were collected after a 3 h incubation because the principal conformational changes of Aβ$_{1-42}$ have been found at this incubation time [26]. The data were corrected by subtracting the spectra of a sample that contained all of the components except Aβ$_{1-42}$. The data were converted to mean residue ellipticity and analyzed using the Selcon [32] and K2D programs [33] to calculate the predominance of secondary structures.

AFM

For visualization of Aβ$_{1-42}$ alone or in presence of the compounds, 5 μl of a 50 μM Aβ$_{1-42}$ peptide solution in the absence or presence of the selected compounds (100 μM) was incubated for 24 h, deposited onto glass slides and dried.

To determine whether the incubation of Aβ$_{1-42}$ (50 μM) in presence of the best compound (100 μM) favors the formation of oligomers, 5 μL samples at 0, 1, 5 and 17 h of incubation at 37°C with shaking were collected, deposited onto glass slides and dried. In addition, samples of Aβ$_{1-42}$ alone at the same incubation times were obtained to compare the results. All of the images were scanned in air by AFM (MultiMode V; Veeco, USA) using the tapping mode.

Determination of IC$_{50}$ of Aβ$_{1-42}$ fibrillation by ThT fluorescence

Once the Aβ$_{1-42}$ aggregation inhibitor activities were corroborated, the IC$_{50}$ for the best compounds were determined as described below. After 24 h of incubation of Aβ$_{1-42}$ (50 μM) with one of several concentrations of the selected compounds (0.001, 0.1, 1, 10, and 100 μM), the inhibition of Aβ$_{1-42}$ fibrillization was measured using the ThT assay, as described above.

Frontier orbitals.

Additional *in silico studies* were performed to determine the molecular basis of the recognition of Aβ$_{1-42}$ by the best compounds because these studies provide electronic details regarding the compounds' effects on Aβ$_{1-42}$ conformational changes. The geometry of the ligands, the Aβ$_{1-42}$ peptide and the ligand–Aβ$_{1-42}$ complexes were fully optimized using the AM1 all-valence

electron self-consistent field molecular orbital approximation [34]. This method is included in the Gaussian 2009 package of programs [35] with default parameters.

The HOMO, SOMO and LUMO energies [36] were determined for the structures obtained after interacting with the **Aβ-α**, **Aβ-RC** and **Aβ-β** peptides to understand their interaction with the peptide site. Molecular electrostatic potential maps (MEPs) [37] were obtained for the ligands to complete the electronic analysis. All of the geometric and electronic calculations were performed using the Gaussian 09 package of programs [36].

Results

Ligand selection

Most of the ligands that inhibit Aβ$_{1-42}$ oligomerization had an amine, which is capable of acquiring a positive charge at pH 7.4, and an aromatic ring [10–12]. Therefore, we chose 26 compounds from the Sigma–Aldrich database (http://www.sigmaaldrich.com) with these chemical characteristics (Fig 1). ACh, which contains a quaternary amine, was selected as a reference ligand to evaluate the influence of the lack of an aromatic group on the recognition on Aβ$_{1-42}$ (Fig 1; compound 26). The protonation states (pKa values) of the amine in the compounds were considered based on the ionizable groups at physiological pH.

Docking studies

We employed three Aβ$_{1-42}$ conformations to perform docking studies. The first conformer corresponded to the 1Z0Q structure obtained from the PDB, which corresponds to the classical α-helical conformation of Aβ$_{1-42}$. According to the stride server, 43% of the residues were in the α-helix conformation. This conformer was labeled **Aβ-α**. The second conformer corresponded to the Aβ$_{1-42}$ conformation obtained at 10 ns in the MD simulations, as reported in a previous work [26]. This conformer represents the RC, according to the determination of its secondary structure by the stride server (**Aβ-RC**; 90% random coil and 10% turn). The last conformer corresponded to an Aβ$_{1-42}$ monomer from the 2BEG structure obtained from the PDB, which has a strand-loop-strand structure similar to what is observed in the mature Aβ$_{1-42}$ fibrils. This conformer was labeled **Aβ-β** (43% β-sheet, 19% turn). The Aβ$_{1-42}$ structures employed were chosen because the principal conformation of Aβ$_{1-42}$ in the membrane is the α-helix [38]. However, in solution, Aβ$_{1-42}$ can adopt different conformations, such as RC, a β-strand structure, and stable turns and bends. In addition, there are several reported conformational changes that occur during aggregation. Both the random coil to β-sheet and α-helix to β-sheet transitions occurred during Aβ folding and assembly. Importantly, the α-helix to β-strand transitions play a prominent role in the fibril assembly process [38].

The twenty-six ligands could be grouped into three families according to their chemical structures. The first group of ligands possessed an amine group that can acquire a positive charge at pH 7.4 and is capable of forming electrostatic interactions with Glu22 and Asp23 (Fig 1; compounds 1, 3–8, 11, 12, 17, 20 and 23–25). The second group consisted of molecules with an amino group covalently coupled to an aromatic ring (Fig 1; compounds 16, 18 and 19). The third group consisted of compounds that had an amine as part of their amide group (Fig 1; compounds 2, 9, 10, 13–15, 21 and 22). These amine groups are capable of forming hydrogen bonds with Glu22 and Asp23. In addition, we included ACh (Fig 1; compound 26) in the *in silico* studies to determine its selectivity for **Aβ-α**, **Aβ-RC** and **Aβ-β** because ACh contained a quaternary amine without an aromatic ring.

Compounds in the first group acted as Lewis bases, which could be protonated at physiological pH [39]. These docking results showed that the compounds formed electrostatic interactions with the carboxylate group of Glu22 and/or Asp23 residues of **Aβ-α** with high affinity

Table 1. Amino acid residues of Aβ$_{1-42}$ that interact with the compounds and their ΔG values obtained via docking studies.

Ligand	Aβ-α		Aβ-RC		Aβ-β	
	ΔG (Kcal/mol)	a.a	ΔG (Kcal/mol)	a.a	ΔG (Kcal/mol)	a.a
1	-5.5	Asp23, Ser26, Asn27	-4.5	Lys28, Gly29, Ala30, Ile31	-3.6	Lys28, Gly29, Ala30, Ile31
2	-4.4	Lys16, Phe20, Asp23, Ile31, Leu34, Met34	-4.5	Gly29, Ala30, Ile31, Ile32	-3.6	Gly29, Ala30, Ile31, Ile32
3	-5.4	Phe19, Asp23, Val24, Lys28, Leu34	-4.5	Phe19, Asp23, Val24, Lys28, Leu34	-3.4	Phe19, Asp23, Val24, Lys28, Leu34
4	-5.8	Gln15, Lys16, Phe19, Asp23	-4.4	Val18, Asp23, Gly25	-3.7	Val18, Asp23, Gly25
5	-6.2	Lys16, Phe19, Phe20, Glu22, Asp23, Asn27	-4.4	Val18, Phe19, Glu22, Asp23	-3.6	Ala21, Gly29, Ala30
6	-5.3	Phe19, Phe20, Asp23, Ile31, Ile34, Ile35	-4.8	Phe19, Glu22, Asp23	-3.7	Phe19, Glu22, Asp23
7	-5.9	Gln15, Lys16, Phe19, Asp23, Asn27	-4.6	Tyr10, Gln15, Phe20, Met35,	-3.7	Tyr10, Glu11, Gln15, Lys16, Phe20, Met35
8	-5.1	Phe19, Phe20, Asp23	-3.9	Phe19, Gllu22, Asp23	-3.6	Phe20, Gly29, Ala30, Ile31
9	-5.2	Asp23, Ile31	-4.1	Ser26, Ala30, Ile31, Ile32	-3.6	Ser26, Ala30, Ile31, Ile32
10	-4.0	Lys16, Ile31, Met35	-3.8	Ala21, Gly25, Ser26, Ala30, Ile31	-3.5	Ala21, Gly25, Ser26, Ala30, Ile31
11	-4.5	Lys16, Phe19, Phe20, Asp23, Ile31	-4.2	Phe19, Glu22, Asp23	-3.3	Phe19, Glu22, Asp23
12	-5.7	Phe20, Asp23, Ile31, Leu34	-4.5	Ala21, Gly25, Ala30, Ile31	-3.3	Ala21, Gly25, Ala30, Ile31,
13	-4.2	Phe19, Glu22, Asp23, Ser26, Asn27,	-4.3	Asp23, Ser26, Lys28, Gly29, Ile31	-3.4	Asp23, Ser26, Lys28, Gly29, Ile31
14	-5.0	Phe2, Phe19, Ile31	-3.9	Hys14, Phe19, Glu22, Asp23	-3.8	Gly29, Ala30, Ile31
15	-4.0	Phe19, Phe20, Gln15, Lys16, Asp23	-4.6	Ala21, Gly29, Ala30, Ile32	-4.2	Ala21, Gly29, Ala30, Ile32
16	-4.3	Val24, Lys28, Ile31, Ile32	-4	Lys16, Asp23, Gly25, Gly29	-3.1	Asp23, Gly25, Gly29, Ala30,
17	-4.1	Val24, Lys28, Ile31, Met35	-4.1	Val24, Ser26	-3.4	Val24, Ser26
18	-5.3	Val24, Lys28, Ile31, Phe20, Ile32	-4.1	Ala21, Gly25, Gly29, Ile31	-3.6	Ala21, Gly25, Gly29, Ile31
19	-4.1	Lys28, Ile31, Val24, Phe20	-4	Val18, Phe19, Glu22	-3.1	Phe20, Ala21, Leu34
20	-4.6	Phe19, Phe20, Asp23, Ile31, Leu34	-4	Hys14, Phe19, Glu22, Asp23	-3.3	Hys14, Phe19, Glu22, Asp23
21	-3.8	Asp23, Ile31, Met35	-4	Gly25, Gly29, Ala30, Ile31, Ile32	-3	Gly25, Gly29, Ala30, Ile31, Ile32
22	-3.7	Gln15, Phe19, Phe20, Asp23, Ile31	-4.5	Ala21, Gly29, Ala30, Ile31, Ile32	-3.7	Ala21, Gly29, Ala30, Ile31, Ile32
23	-5.3	Phe19, Phe20, Asp23, Asn27	-5	Asp23, Val24, Ser26	-3.1	Asp23, Val24, Ser26
24	-5.9	Phe19, Phe20, Asp23, Asn27,	-3.8	Ala21, Glu22, Ala30, Ile31	-3.2	Ala21, Glu22, Ala30, Ile31
25	-5.9	Lys16, Phe19, Phe20, Asp23	-4	Hys14, Val18, Phe19, Asp23	-3.7	Hys14, Val18, Phe19, Asp23
26	-3.6	Phe19, Ala21, Asp23	-4.3	Lys16, Leu17, Phe19	-4	Lys16, Leu17, Phe19

and consequently showed lower ΔG values (Table 1) than **Aβ-RC** and **Aβ-β**. However, according to the theoretical docking studies, this was not the rule in all of the ligands tested.

Although 60% of the selected molecules had these characteristics, the neighboring substituents of each compound modified the binding mode and consequently the ΔG values of Aβ$_{1-42}$.

According to the docking studies, all of the compounds generally showed less affinity to **Aβ-β** than to **Aβ-α** and **Aβ-RC** (Fig 2A), as has been recently reported [40]. In addition, despite
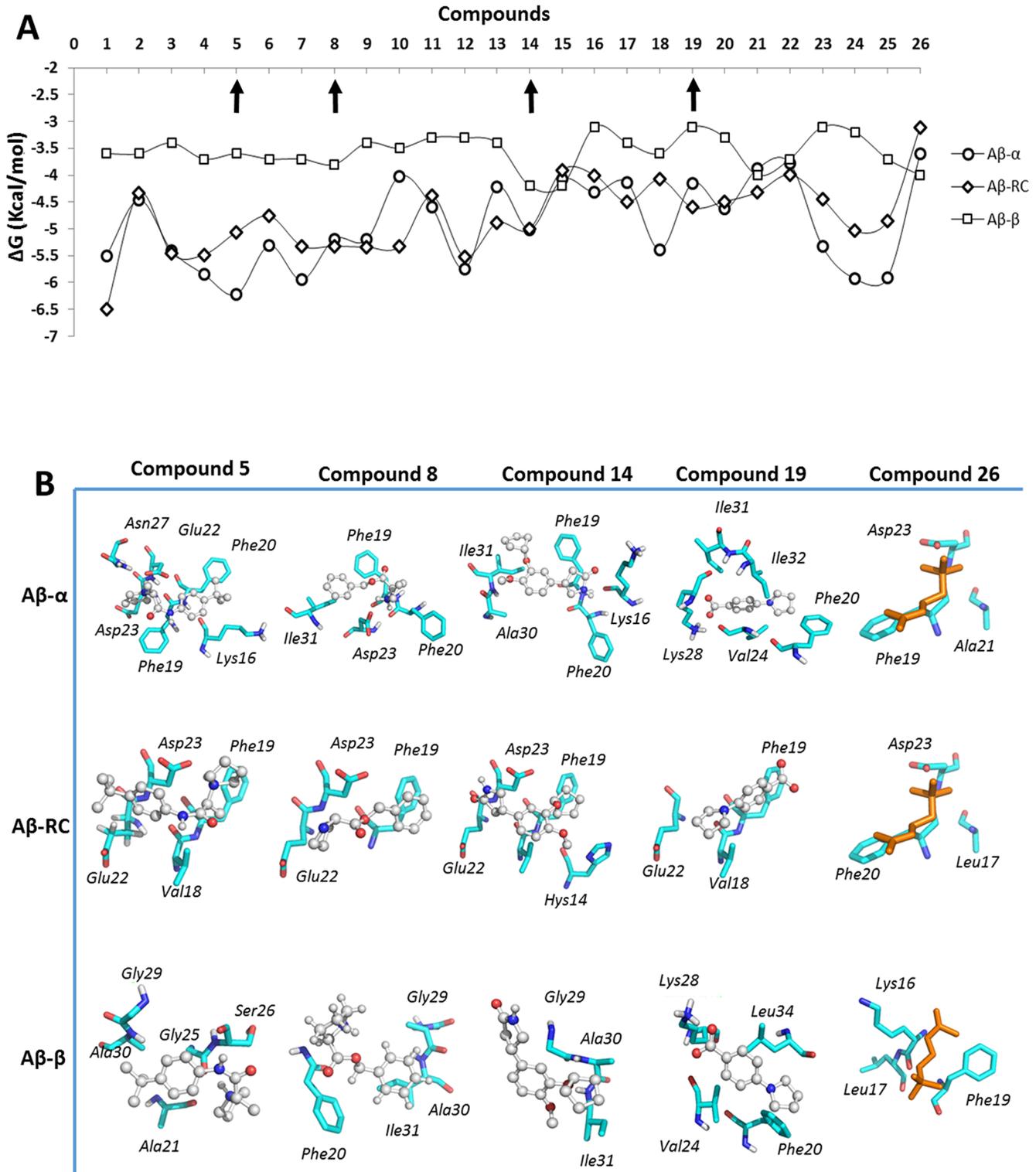
Fig 2. Docking results for the selected compounds with several Aβ$_{1-42}$ conformers. ΔG values were obtained through docking studies of the ligands with **Aβ-α** (circles), **Aβ-RC** (rhombuses) and **Aβ-β** (squares) (A). The binding modes of compounds 5, 8, 14, 21 and 26 on **Aβ-α**, **Aβ-RC**, and **Aβ-β** (B).

doi:10.1371/journal.pone.0130263.g002

several structural differences between the compounds, the ΔG values tended to be similar for all of the compounds obtained in the docking studies with **Aβ-β** and **Aβ-RC**, varying only slightly between the best and the worst compounds (1.0 Kcal/mol). Interestingly, the principal differences in the ΔG values were obtained from the docking studies with **Aβ-α**. Therefore, this result was employed as the starting point for choosing four ligands: one compound with the highest affinity for **Aβ-α** (compound 5); two compounds that showed similar affinities for **Aβ-α** and **Aβ-RC** (compounds 8 and 14); and one compound that showed higher affinity to **Aβ-RC** than **Aβ-α** (compound 19).

The docking analyses showed that the protonated amino group (tertiary amine) of compound 5 binds to the carboxylate groups of Glu22 and Asp23 of **Aβ-α** by electrostatic interactions, whereas the aromatic ring of compound 5 interacted with the lateral chain of Phe19 and Phe20 via π–π interactions. The tert-butyl group of compound 5 interacted with the methylene of Lys16 ([Fig 2B](#)) through hydrophobic interactions. Similarly, compound 5 bound to **Aβ-RC** via electrostatic interactions with Asp23 and Lys28, π-π interactions with Phe19 and hydrophobic interactions with Val18, as shown in [Fig 2B](#). On the other hand, compound 5 interacts with Gly25, Ala21, Gly29 and Ala30 in **Aβ-β** via hydrophobic interactions, resulting in the highest ΔG value for this compound ([Fig 2B](#)).

Compounds 8 and 14 bound to both **Aβ-α** and **Aβ-RC** with similar ΔG values, though these values were lower for compound 8. The protonated amine of compound 8 interacted with the lateral chain of Asp23 via electrostatic interactions, and its aromatic ring formed π–π interactions with the lateral chains of Phe19 and Phe20 in **Aβ-α** ([Fig 2B](#)). Interestingly, compound 8 interacted with Asp23 and Glu22 on **Aβ-RC** via electrostatic interactions while maintaining π–π interactions with the lateral chain of Phe19, and the other interactions were lost ([Fig 2B](#)). The recognition of **Aβ-β** by compound 8 was preserved primarily by hydrophobic interactions with Gly29 and Ile31 ([Fig 2B](#)), and its aromatic ring interacted with Phe20 in the lateral chain. Compound 14 formed hydrophobic interactions with the lateral chain of Ile31 and Ala30 as well as π–π interactions with the lateral chains of Phe19 and Phe20 in **Aβ-α** ([Fig 2B](#)). These interactions were preserved between compound 14 and **Aβ-β** ([Fig 2B](#)). Compound 14 could establish hydrogen bond interactions with Glu22 and Asp23 on **Aβ-RC** as well as a π–π interaction with Phe19, as can be observed in [Fig 2B](#).

Compound 19 lacked a protonated tertiary amine, forming only hydrogen bonds, similar to compound 14. Furthermore, it did not interact with the carboxylate groups of Glu22 and Asp23. However, the carboxylate group of compound 19 interacted with the lateral chain of residue Lys28 via electrostatic interactions, while its aromatic ring interacted with the lateral chain of residue Phe20 via π–π interactions and with the lateral chains of residues Val24, Ile31 and Ile32 in **Aβ-α** via hydrophobic interactions ([Fig 2B](#)). In contrast, compound 19 interacted with **Aβ-RC** via hydrophobic interactions with Val18, Phe19, and Glu22 ([Fig 2B](#)). Compound 19 interacted with the side chain of Phe20 through π–π interactions and with Leu34 and Val24 via hydrophobic interactions, while preserving the electrostatic interaction with Lys28 ([Fig 2B](#)).

For comparison, the quaternary amine of ACh interacted with the lateral chain of Asp23 via electrostatic interactions and formed hydrophobic interactions with Phe19 ([Fig 2B](#)). This binding mode was preserved in the interaction of ACh with **Aβ-RC**. ACh did not interact with Asp23 in **Aβ-β**, and the principal non-binding interactions established between ACh and **Aβ-β** were hydrophobic interactions with Leu17 and Phe19 ([Fig 2B](#)). The higher ΔG values exhibited by ACh led us to infer that the lack of an aromatic ring was responsible for these results, although the formation of electrostatic interactions between the tertiary amine of ACh and the lateral chain of Asp23 in **Aβ-α** were preserved.
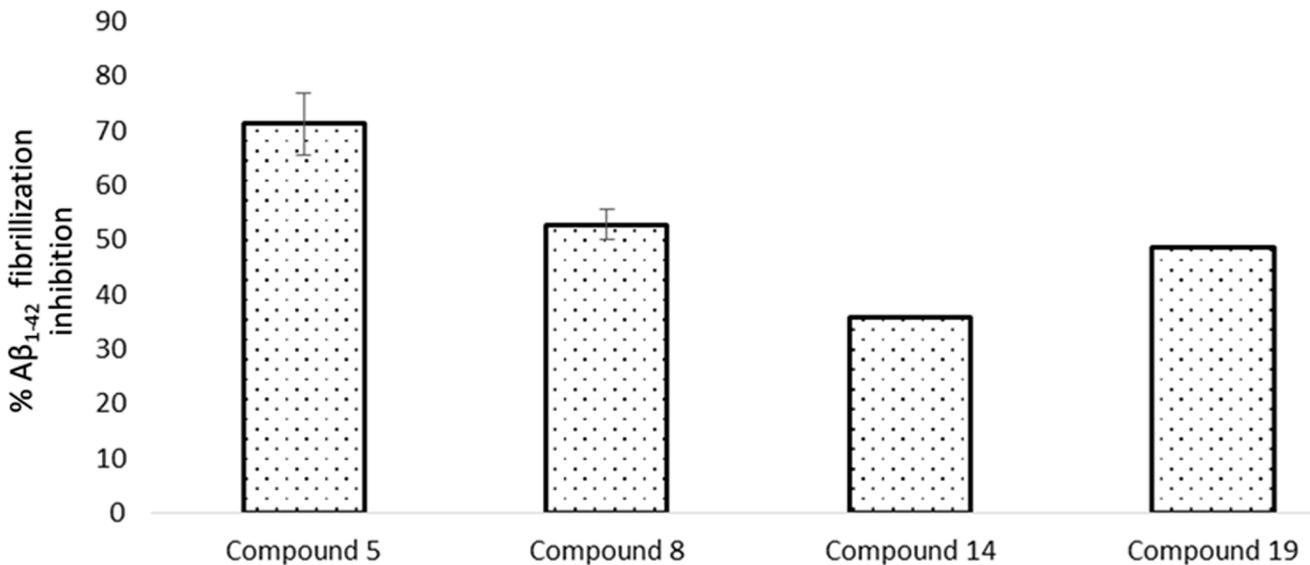
Fig 3. Results of the ThT fluorescence assay showing the effects of the selected compounds on the Aβ$_{1-42}$ fibrillization process. Aβ$_{1-42}$ (50 μM in MilliQ water) was incubated at 37°C in a quartz cell in the presence or absence of compounds 5, 8, 14 and 19 (100 μM) and stirred at 250 rpm for 24 h. The increase in ThT (3.3 μM) fluorescence was measured at the end of the incubation time.

doi:10.1371/journal.pone.0130263.g003

Evaluation of Aβ1–42 aggregation by ThT fluorescence.

In vitro studies were performed to determine whether the selected compounds could affect the pathological aggregation of Aβ$_{1-42}$. For this purpose, a non-fibrillated Aβ$_{1-42}$ peptide was the starting material used to monitor the fibrillization process [26]. The selected compounds inhibited the pathological aggregation of Aβ$_{1-42}$, although compounds 5 and 8 were the best inhibitors. As shown in Fig 3, compound 5 inhibited the formation of Aβ$_{1-42}$ fibrils by 73%, whereas compound 8 inhibited Aβ$_{1-42}$ fibril formation by 53% at the end of the incubation period (24 h).

CD

To determine the secondary structure of Aβ$_{1-42}$ in the presence of the selected compounds, CD studies were performed. The spectra were corrected for the contribution of the CD spectra to the ellipticity of the compounds. After the samples were incubated without the compounds for 3 h under conditions that favored fibril formation, the CD spectra showed changes in the secondary structure, which represented the β-sheet (59.5%) conformation of Aβ$_{1-42}$ (Table 2) [32]. When Aβ$_{1-42}$ was incubated in the presence of compound 5, the CD spectra indicated a high proportion of RC content (56.5%), which resembles the conformation of unordered

Table 2. Proportions of Aβ$_{1-42}$ secondary structures in the absence or presence of 100 μM of the selected compounds.

Sample	α (%)	β-sheet (%)	RC (%)	Error
Aβ$_{1-42}$	2	59.5	38.5	11.5
Aβ$_{1-42}$- compound 5	18.5	15.5	56.5	11.5
Aβ$_{1-42}$- compound 8	11.5	48	40.5	6.5
Aβ$_{1-42}$- compound 14	14.5	52.5	33	11.5
Aβ$_{1-42}$- compound 19	5.5	52	42	11.5

doi:10.1371/journal.pone.0130263.t002

peptides [32]. A significant reduction in the proportion of β-sheet structure (15.5%) was also observed, though there was a small increase in the proportion of α-helix structure (18.5%), as shown in Table 2. Similarly, when $A\beta_{1-42}$ was incubated in the presence of compound 8, the CD spectra indicated a high proportion of RC content (40.5%), though this was similar to the proportion of β-sheet structure (48%). A small increase in the proportion of α-helix structure (11.5%) was observed. For compounds 14 and 19, a high level of β-sheet content (52.5% for 14 and 52% for 19) was observed, although this proportion was lower than $A\beta_{1-42}$ alone (59.5%).

AFM

We used AFM to study the size and morphology of the $A\beta_{1-42}$ aggregates after a 24 h incubation in the presence or absence of the selected compounds. The morphology of the $A\beta_{1-42}$ aggregates in the presence of the selected compounds was different than the morphology of the fibrils obtained with $A\beta_{1-42}$ alone. Fig 4A shows the characteristic fibrils of $A\beta_{1-42}$, which have a width of ~30 nm and a height of ~20 nm. However, incubation of $A\beta_{1-42}$ in the presence of compound 5 favored the formation of amorphous aggregates in which neither fibrils nor oligomeric species were found (Fig 4B).

In contrast, the incubation of $A\beta_{1-42}$ with compounds 8 and 14 resulted in the formation of the characteristic spherical oligomers with a radius of 10–30 nm, as shown in Fig 4C and 4D, respectively. Fibrils were not observed. Additionally, as shown in Fig 4E, the incubation of $A\beta_{1-42}$ with compound 19 resulted in the formation of a spherical species with a radius of 60–80 nm. However, these spheres were larger than the characteristic oligomers shown in Fig 4C and 4D.

To determine whether the incubation of $A\beta_{1-42}$ and compound 5 favored the formation of oligomers prior to the formation of amorphous aggregates, several samples of $A\beta_{1-42}$ alone and in the presence of compound 5 were obtained during different incubation times (0, 1, 5 and 17 h). No $A\beta_{1-42}$ oligomer formation was observed (Fig 4F and 4G).

As shown in Fig 4F, the resuspension of $A\beta_{1-42}$ results in a dense, homogeneous field of unaggregated peptide. In comparison, after 1 h of incubation, the height of the individual peptide structures as measured by AFM was 1.5 nm, which was in agreement with the expected size of a single $A\beta_{1-42}$ monomer. Importantly, after 5 h of incubation, an increase in the formation of protofibrils (>200 nm) was observed. This was more evident after 17 h of incubation, with an increase in the presence of short fibrils (>500 nm).

In comparison, the presence of compound 5 did not alter the morphology of $A\beta_{1-42}$ after 1 h of incubation, as shown in Fig 4G. However, after 5 h of incubation, the monomeric form of $A\beta_{1-42}$ was maintained, and each individual peptide structure was 1.5 nm in height. However, the presence of small amorphous aggregates was observed, which was more evident after 17 h of incubation.

Determination of IC_{50} of $A\beta_{1-42}$ fibrillation by ThT fluorescence

Once compounds 5 and 8 were established as inhibitors of the pathological aggregation of $A\beta_{1-42}$, their IC_{50} values were determined as 1.28 μM (compound 5) and 34.36 μM (compound 8) for use in future assays. Then, to determine how the binding modes of compounds 5 and 8 affected the pathological aggregation of $A\beta_{1-42}$, the electronic behavior and the molecular basis of the recognition of $A\beta_{1-42}$ by these compounds were analyzed using quantum chemistry.

Frontier orbitals

A full geometry optimization was performed using the semi-empirical quantum mechanical program AM1 to calculate the heat of formation. The HOMO, SOMO and LUMO energies
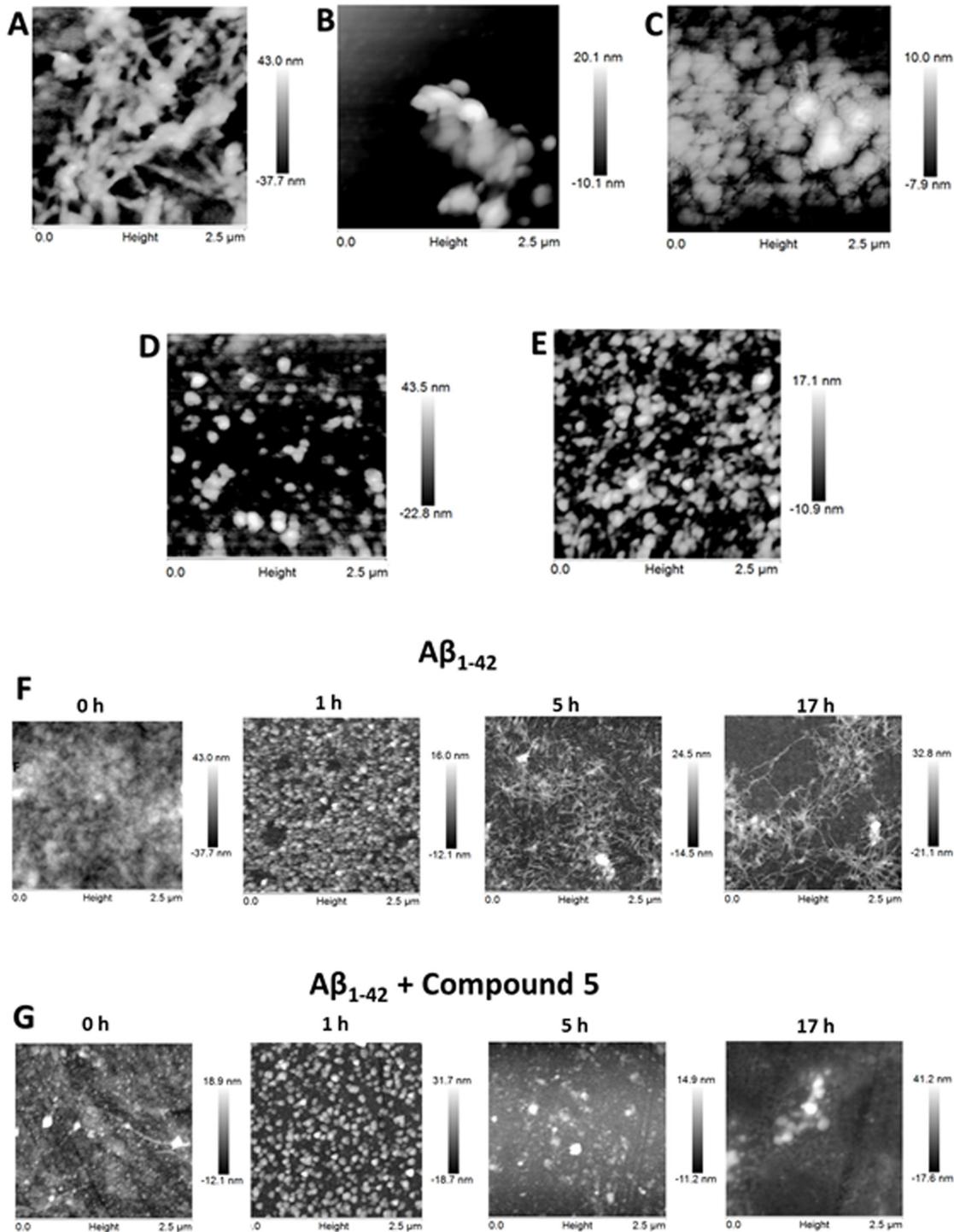
Fig 4. AFM analysis after incubating 50 μM Aβ$_{1-42}$ alone or in the presence of the selected compounds at 100 μM after 24 h (A to E) or different incubation times (F and G). Aβ$_{1-42}$ alone (A); Aβ$_{1-42}$ and compound 5 (B); Aβ$_{1-42}$ and compound 8 (C); Aβ$_{1-42}$ and compound 14 (D); Aβ$_{1-42}$ and compound 19 (E). Samples obtained at different incubation times for Aβ$_{1-42}$ alone (F) or with compound 5 (G). Aβ$_{1-42}$ (50 μM in MilliQ water) was incubated at 37°C in a quartz cell in the presence or absence of compounds 5, 8, 14 and 19 (100 μM) and stirred at 250 rpm for 24 h.

doi:10.1371/journal.pone.0130263.g004

Table 3. Comparison of LUMO, HOMO and SOMO (eV) and the electronic energies of the amino acid residues and compounds.

Structure	LUMO (eV)	HOMO (eV)	SOMO (eV)	Energy (ΔH), Kcal/mol
Aβ-α	-1.3		-8.35	-2309.8
Aβ-RC	-1.17		-7.56	-2176.3
Aβ-β	-0.96		-7.79	-2266.4
Compound 5 (α)	-3.68	-12.24		116.6
Compound 8 (α)	-4.1	-12.3		88.3
Compound 5 (RC)	-3.78	-12.66		117.21
Compound 8 (RC)	-4.1	-12.3		88.28
Compound 5 (β)	-3.83	-12.62		118.0
Compound 8 (β)	-4.1	-12.3		88.3

(α) After docking studies with **Aβ-α**

(RC) After docking studies with **Aβ-RC**

(β) After docking studies with **Aβ-β**

doi:10.1371/journal.pone.0130263.t003

were also determined for the **Aβ-α**, **Aβ-RC** and **Aβ-β** conformations; for the compounds alone; and for the $A\beta_{1-42}$–ligand complexes. Because the Aβ structure was used after the docking studies, it was not possible to obtain the HOMO energy from the presence of unpaired electrons that would indicate interactions with the ligand or whether the electrons were shared or transferred. The SOMO orbital energy of $A\beta_{1-42}$ was obtained and was found to be more negative for **Aβ-α** (Table 3). Therefore, it was possible that the SOMO orbital energy of $A\beta_{1-42}$ could have reacted with the LUMO energy of the ligands. Compounds 5 and 8 may act as inhibitors of $A\beta_{1-42}$ oligomerization because their GAP values showed less of a difference in interaction energy between these two compounds and $A\beta_{1-42}$ (Fig 5A). When the complex was formed between **Aβ-α** and compound 5, the LUMO orbital energy was located in the region where the ligand was recognized (Fig 5B), suggesting electronic interchanges.

The recognition sites of compounds 5 and 8 corresponded to the region where the peptide turned to acquire a U shape (Ala21–Val24), and this was the location where the LUMO orbital energies for compounds 5 and 8 had more negative values (Table 3). Therefore, the interaction between compound 8 and **Aβ-α** was more favorable.

However, although compound 8 has the same recognition site for $A\beta_{1-42}$ as compound 5, compound 8 did not prevent a conformational change in $A\beta_{1-42}$. This could be due to the interaction maintained by each compound.

In addition, the interaction energy of compound 5 with **Aβ-α** (ΔE kcal/mol -50.29) was more stable than that of compound 8 (ΔE kcal/mol 3.49). This energy could explain why compound 5 had better ΔG values in the docking studies. Table 3 shows the ΔH values for compounds 5 and 8, which verified that the conformation of compound 5 alone was not the most stable, but it was stabilized when it complexed with $A\beta_{1-42}$. This did not occur for compound 8.

To predict the behavior and reactivity of the molecules, the MEP was also obtained. MEP has largely been used as a molecular descriptor of chemical reactivity in many biological systems because it allows for visualization of the electrophilic and nucleophilic sites in a molecule [41]. In the MEP maps, there are three important colors that are used to indicate the value of the electrostatic potential: blue (positive), red (negative) and green (no charge). The surfaces with green colors indicate zero potential. As shown in Fig 3D–3G, compounds 5 and 8 had electronegative zones that were associated with the pair of electrons corresponding to the
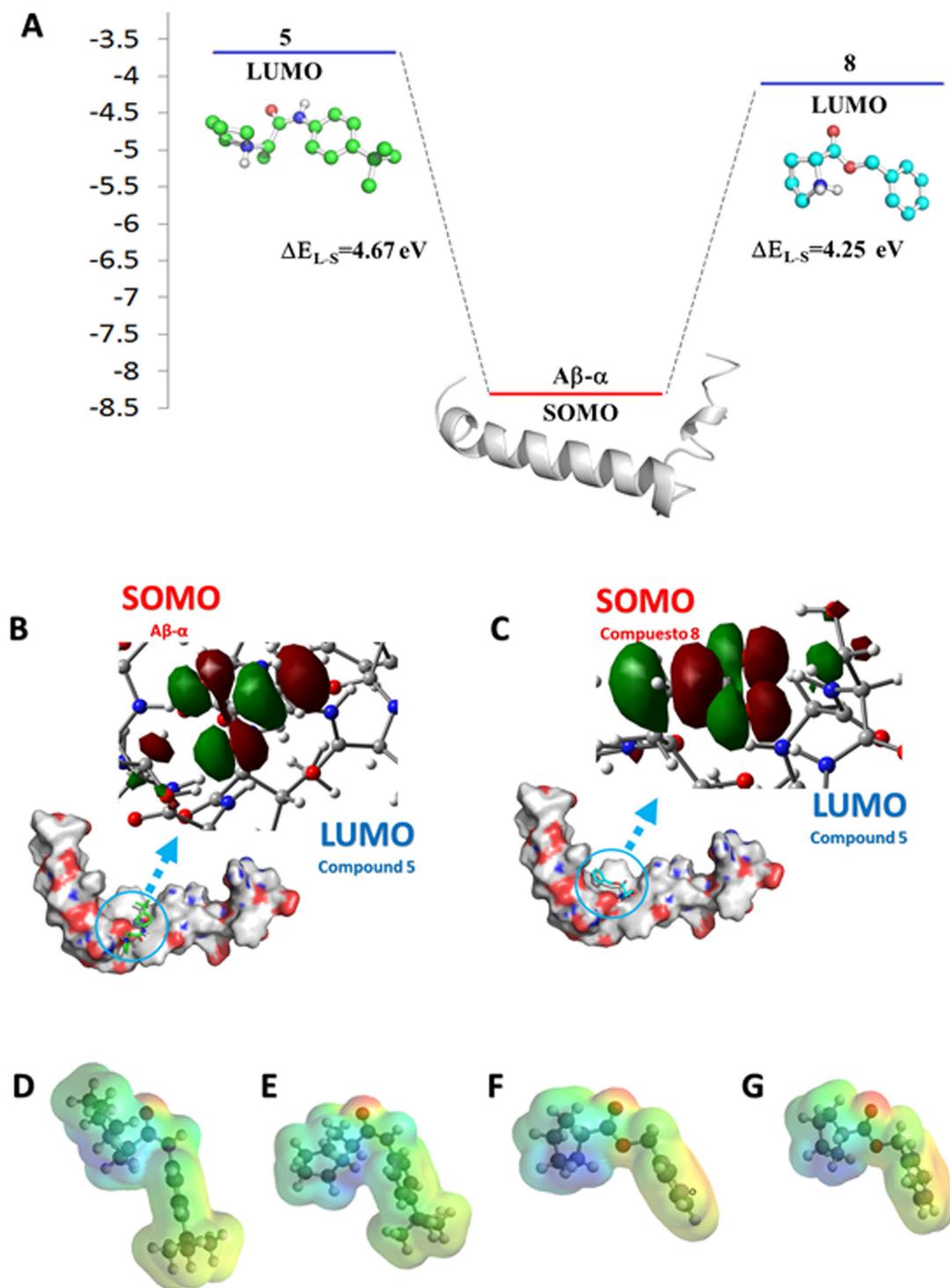
Fig 5. Spatial distribution of SOMO on Aβ-α. The illustration is based on the mapping of 0.032 isovalues and values onto a total electron density surface contoured at 0.0004 e/au3, which was based on AM1 semi-empirical calculations. The interaction between the LUMOs of compounds 5 and 8 and the SOMO of Aβ-α, in eV (A); Aβ-α–compound 5 complex SOMO (B); and Aβ-α–compound 8 complex SOMO (C) are shown. A map of the electrostatic potentials showing the most positive potential (deepest blue color) and the most negative potential (deepest red color) plotted on a surface with constant electron density (0.02 e/au3). MEP for compound 5 after docking studies with Aβ-α (D); MEP for compound 5 after docking studies with Aβ-β (E); MEP for compound 8 after docking studies with Aβ-α (F); and MEP for compound 8 after docking studies with Aβ-β (G).

doi:10.1371/journal.pone.0130263.g005

oxygen atoms. The positive electrostatic potentials were located at the acidic hydrogen atoms of the amine group.

Therefore, the GAP and MEP indicated that compounds 5 and 8 could be oligomerization inhibitors, but the interaction energy and conformational changes induced in **Aβ-α** by interaction with the ligands suggested that compound 5 was a better inhibitor than compound 8. Compound 5 exhibited different conformations when interacting with **Aβ-α** and **Aβ-β**, whereas compound 8 had the same conformation for both **Aβ-α** and **Aβ-β**. Compound 8 had more sites with free movement than compound 5 due to its bonds with sp^3 hybridization, which could explain the conformations obtained in the docking experiments with compound 5. In particular, the hydrogen atom of the quaternary amine of compound 5 formed a double hydrogen bond with a carboxyl group of the peptide at distances of 2.17 and 1.87 Å, which indicated a strong interaction. Perhaps, this group could have indirectly encouraged the other interactions describing by the docking studies due to the volume of the isobutyl substituent.

Similarly, the interaction energy of compound 5 with **Aβ-RC** (ΔE kcal/mol -42.1) was more stable than that of compound 8 (ΔE kcal/mol -30.5). Table 3 shows the ΔH values for compounds 5 and 8, which verified that the conformation of compound 5 alone was not the most stable, but it was stabilized when it complexed with $A\beta_{1-42}$. This did not occur for compound 8 and is similar to the behavior observed with **Aβ-α.**

In contrast, the interaction of compound 5 with **Aβ-β** showed a more extended conformation that did not provoke any conformational changes in $A\beta_{1-42}$. A different conformation was obtained for each ligand. For instance, the interaction between **Aβ-α** or **Aβ-RC** and compound 5 favored the exposure of some atoms, such as the interaction between the hydrogen atom of the quaternary amine of the ligand and the oxygen atom of the carboxylic group of $A\beta_{1-42}$. However, when compound 5 interacted with **Aβ-β**, its conformation was different, even though the distribution of the positive and negative electrostatic potential of the compound 5 was located in the same region of the molecule. According to the quantum results (AM1), the conformation of compound 5 in the interaction with **Aβ-β** was similar to that observed for compound 8 in both conformations of $A\beta_{1-42}$. This showed the presence of intermolecular interactions via hydrogen bonding between the hydrogen atoms of the quaternary amino group and the amide or the carboxylic groups of the peptide.

Discussion

The relationship between the pathological aggregation of $A\beta_{1-42}$ and AD implies that the $A\beta_{1-42}$ aggregation inhibitors should be able to slow disease progression [42–46]. The development of compounds with high affinity to the α-helix conformation could block the adoption of the β-sheet conformation by interacting with Asp23 or Lys28 and preventing the formation of the required salt bridge during the $A\beta_{1-42}$ oligomerization process [21].

Although a wide variety of organic compounds have been shown to inhibit $A\beta_{1-42}$ aggregation (Fig 6) [10–15], many of them cannot be used because they are cytotoxic in cultured cells, favor the formation of oligomeric species, or have low bioavailability due to high molecular weights (>500 g/mol), which makes it difficult for them to cross lipid layers [42]. Because the cytotoxicity and genotoxicity of curcumin has been demonstrated in some cultured cells [47], several chemical analogs have been designed to overcome these limitations [12]. In addition, the activity of 1,2,3-hydroxyl-*scyllo*-inositol (Fig 6) as a fibril-forming inhibitor has been demonstrated by ThT fluorescence and AFM [15]. However, these compounds favor the formation of oligomeric species, which could result in toxic effects because of the correlation between the levels of soluble oligomers (rather than insoluble $A\beta_{1-42}$ fibrils) and the extent of synaptic loss and cognitive impairment [48–51].
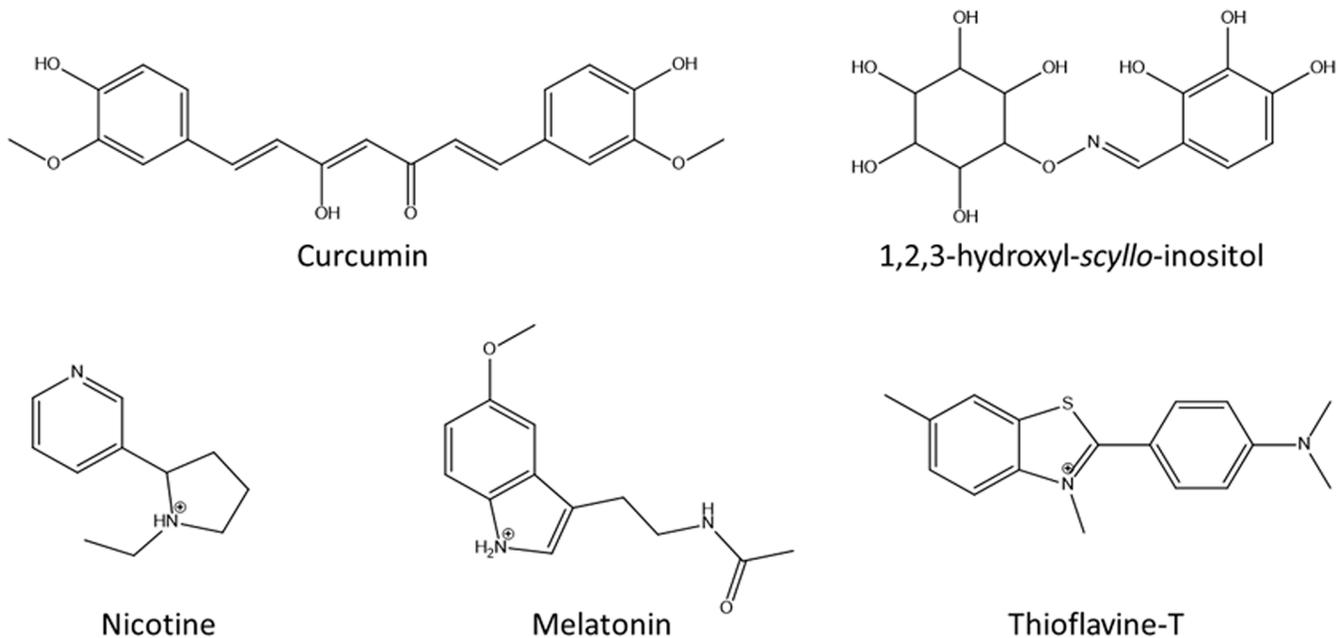
Fig 6. Chemical structures of the inhibitors of Aβ$_{1-42}$ fibrillization. The majority of the compounds shared the presence of amines and/or aromatic rings.

Melatonin and ThT have been shown be to inhibit Aβ$_{1-42}$ fibril formation. These compounds share the presence of aromatic rings and protonated amines. These are important chemical characteristics for the recognition of Aβ$_{1-42}$ because BTA-1, a neutral analog of ThT, is ineffective in inhibiting Aβ$_{1-42}$ fibril formation [52].

Recently, NMR studies have demonstrated that 1,4-naphthoquinon-2-yl-L-tryptophan, which has been reported to reduce the level of aggregation and toxicity of Aβ$_{1-42}$, could interact with Phe20, Ala21, Glu22, Val18 and Val24 [53, 54], demonstrating that the presence of a positive group and an aromatic ring are important for the recognition of the turn region in Aβ$_{1-42}$.

The majority of the Aβ$_{1-42}$ aggregation inhibitors mentioned above share tertiary amines and aromatic rings. This was taken into account when we selected 26 compounds with MW < 500 g/mol that each contain an amine group and an aromatic ring. After analysis of the *in silico* results, four ligands (compounds 5, 8, 14 and 19) were selected to evaluate their effects on Aβ$_{1-42}$ oligomerization and the changes to its secondary structure. The four ligands included one with the highest affinity to **Aβ-α** (compound 5); two compounds that showed a similar affinity to **Aβ-α** and **Aβ-RC** (compounds 8 and 14); and one that showed a higher affinity to **Aβ-RC** than the **Aβ-α** conformation (compound 19).

The results of the *in silico* studies showed that compound 5 had the best affinity for **Aβ-α**, which explains its ability to inhibit the pathological aggregation of Aβ$_{1-42}$. This resulted in the loss of ThT-positive Aβ$_{1-42}$ β-sheets. The CD studies demonstrated the absence of the β-sheet conformation and the predominance of the RC structure, which indicates an unordered peptide conformation.

These results were mirrored by the AFM results, which showed structural changes in the Aβ$_{1-42}$ deposits from the characteristic fibrils to amorphous precipitates when compound 5 was present (compound 5: Aβ$_{1-42}$ ratio 2:1). This pattern of oligomerization inhibition is similar to that reported for copper [52]. By incubating Aβ$_{1-42}$ in the presence of 200 μM copper under fibril-forming conditions, the appearance of fibrils decreased, and non-fibrillary, amorphous aggregates increased [52]. The formation of amorphous aggregates could represent a

beneficial characteristic because recent evidence suggests that most of the detrimental forms of $A\beta_{1-42}$ are soluble oligomers, whereas insoluble amorphous aggregates represent a less harmful, inactivated form of $A\beta_{1-42}$ [51].

In contrast to the results mentioned above, although compound 8 had a positively charged group and an aromatic ring similar to compound 5, the absence of linearity did not provide a favorable arrangement of these functional groups. This structural difference completely changed the binding mode of compound 8. Nevertheless, the GAP results indicated that compound 8 could react better with $A\beta_{1-42}$. In addition, the lack of hydrophobic substituents on the aromatic ring prevented the hydrophobic interactions with the methylene group of Lys16.

Although compounds 8 and 14 exhibited similar affinities for both conformations of $A\beta_{1-42}$, these compounds were only capable of reducing the ThT fluorescence by 50%. These results are in agreement with the AFM observations, which showed the formation of the characteristic oligomer species that are related to neurotoxicity [9]. Although compound 14 established several hydrophobic and π–π interactions, the lack of ionizable groups diminished its ability to bind to homologous amino acids, resulting in its high binding energy.

The carboxylate group of compound 19 interacted with the side chain of Lys28, which may have prevented the formation of the salt bridge. However, the presence of the aromatic rings did not provide selectivity for **Aβ-α**, even though the turn portion (amino acid residues 27–30) showed fewer conformational changes during oligomerization in comparison with the β1 portion (amino acid residues 18–26) [22]. Compound 19 was only able to reduce ThT fluorescence for $A\beta_{1-42}$, with similar proportions of β-sheet and RC conformations. The $A\beta_{1-42}$ aggregates in the presence of compound 19 were similar to the spherical oligomer species produced by compounds 8 and 14, but with a higher ratio.

According to the results obtained above, oligomer formation can result when the compounds are able to bind the β-sheet and α-helix conformations with similar, rather than greater, ΔG values for $A\beta_{1-42}$. Furthermore, because of the toxicity of these oligomers, it is necessary to prevent this event [10, 48].

Peptide structures that can interact with the negative region of $A\beta_{1-42}$ (Glu22 and Asp23) have been proposed to be a useful alternative for the design of oligomerization inhibitors [55]. According to the results obtained, it can be noted that blocking the formation of the salt bridge only is insufficient to prevent $A\beta_{1-42}$ oligomerization. In fact, several molecules have demonstrated this pattern of $A\beta_{1-42}$ inhibition.

For these reasons, several chemical moieties are necessary for the preferential recognition of **Aβ-α** and must have a linear spatial arrangement that allows for interaction with residues 13–26, which are implicated in **Aβ-α** stabilization [20].

As shown in Fig 7A, the principal type of interactions that drive the selectivity of **Aβ-α** are electrostatic interactions with residues Glu22 and Asp23 and π–π interactions with Phe19 and Phe20. The formation of π–π interactions indicates the presence of an important moiety because the formation of strong π–π interactions between these chemical groups has been demonstrated to represent an intermediary stage in the unfolding process that drives the adoption of the β-sheet conformation [56].

The distance between both groups is important. Docking studies have shown that molecules with a distance of 4.3–5 Å between the amine and aromatic groups (Fig 7B) have selectivity for **Aβ-α** (4–7,11,12,24,25). However, the ΔG values vary considerably because the aromatic rings of the different compounds represent different substituents, and the presence of aliphatic substituents or aromatic rings favors the recognition of **Aβ-α**. The presence of polar or charged groups in the compounds increases the ΔG values, and consequently, the affinity. These characteristics are consistent with the design of curcumin derivatives, in which the presence of aryl
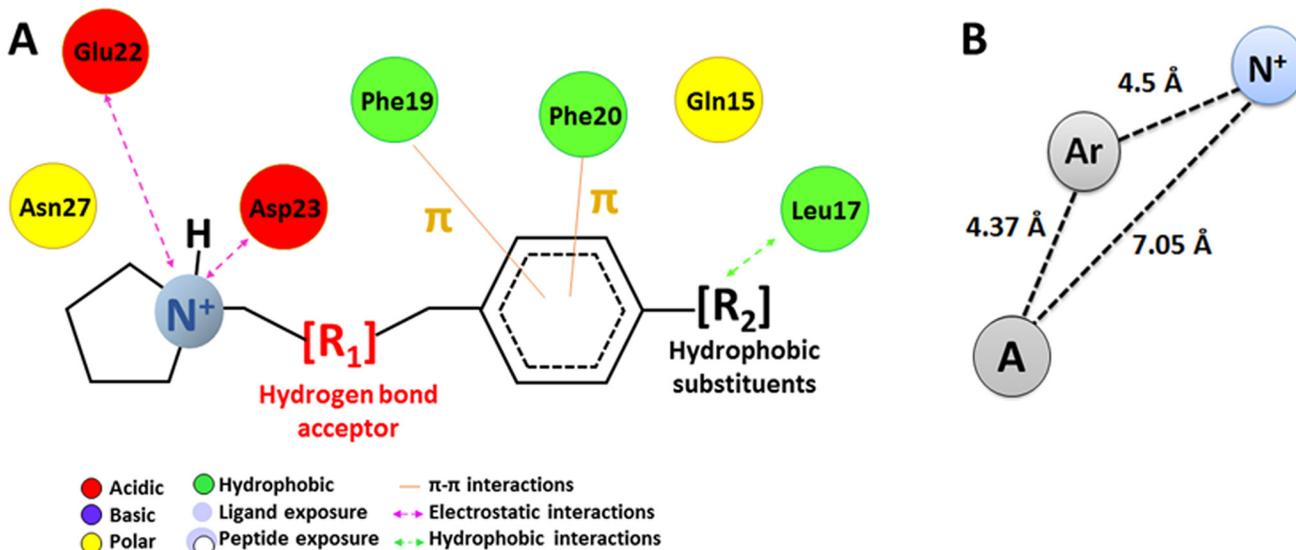
Fig 7. Proposed Aβ-α pharmacophore based on the studies with compound 5. Schematic representation of the polar and nonpolar interactions that favor the interactions with **Aβ-α** (A); distances between principal chemical groups, the protonated amine (N⁺), the aromatic ring (Ar), and Alkyl substituent (*Tert-B*) (B). The main interactions involved in the recognition of compound 5 are electrostatic interactions with Glu22 and Asp23, π-π with Phe19 and Phe20 and hydrophobic interactions with Leu17.

rings with methoxy substituents are necessary for improving the inhibitory activity of curcumin [14].

Note that several drugs have these same characteristics, as was reported for melatonin [12]. Additionally, nicotine, a potent parasympathomimetic alkaloid, has shown the capability to retard amyloidosis by preventing α-helix to β-sheet conformational transformation, an event that is important in the pathogenesis of Alzheimer's disease [11]. Moreover, nicotine has an aromatic ring and a tertiary amine that are capable of acquiring a positive charge at physiological pH.

The tricyclic antidepressant amitriptyline showed a significant potentiation of the non-toxic Aβ monomer with a concomitant decrease in the cytotoxic dimer Aβ load in triple transgenic mice [57]. This suggests that amitriptyline has a similar mechanism of action for $Aβ_{1-42}$ aggregation inhibition. However, the multiple adverse effects of amitriptyline, such as nausea, psychosis, constipation, blurred vision, heart rhythm disorders, postural hypotension and extrapyramidal symptoms, prevent its long-term use. Galantamine, an AChE inhibitor, has shown concentration-dependent inhibition of both $Aβ_{1-40}$ and $Aβ_{1-42}$ aggregation [58].

In addition, note that the compounds mentioned previously show similar interactions with the conformers of Aβ as compound 5. As shown in Fig 8, curcumin, melatonin and ThT exhibit higher affinity for **Aβ-α** and **Aβ-RC** than **Aβ-β** and importantly establish interactions with Glu22, Asp23, Phe19, Gln15, Lys17, Leu17 and Asn27 as shown for compound 5 on **Aβ-α** and **Aβ-RC**.

Conclusion

These results show that compounds with different selectivities for the α-helix and β-sheet conformations of $Aβ_{1-42}$ have different inhibitory effects on $Aβ_{1-42}$ aggregation. Compounds with a higher affinity for **Aβ-α** could prevent the formation of the oligomeric species, whereas compounds with a higher affinity for the **Aβ-β** conformation allowed their formation. In particular, some chemical reactions were necessary for the preferential recognition of **Aβ-α**, including the
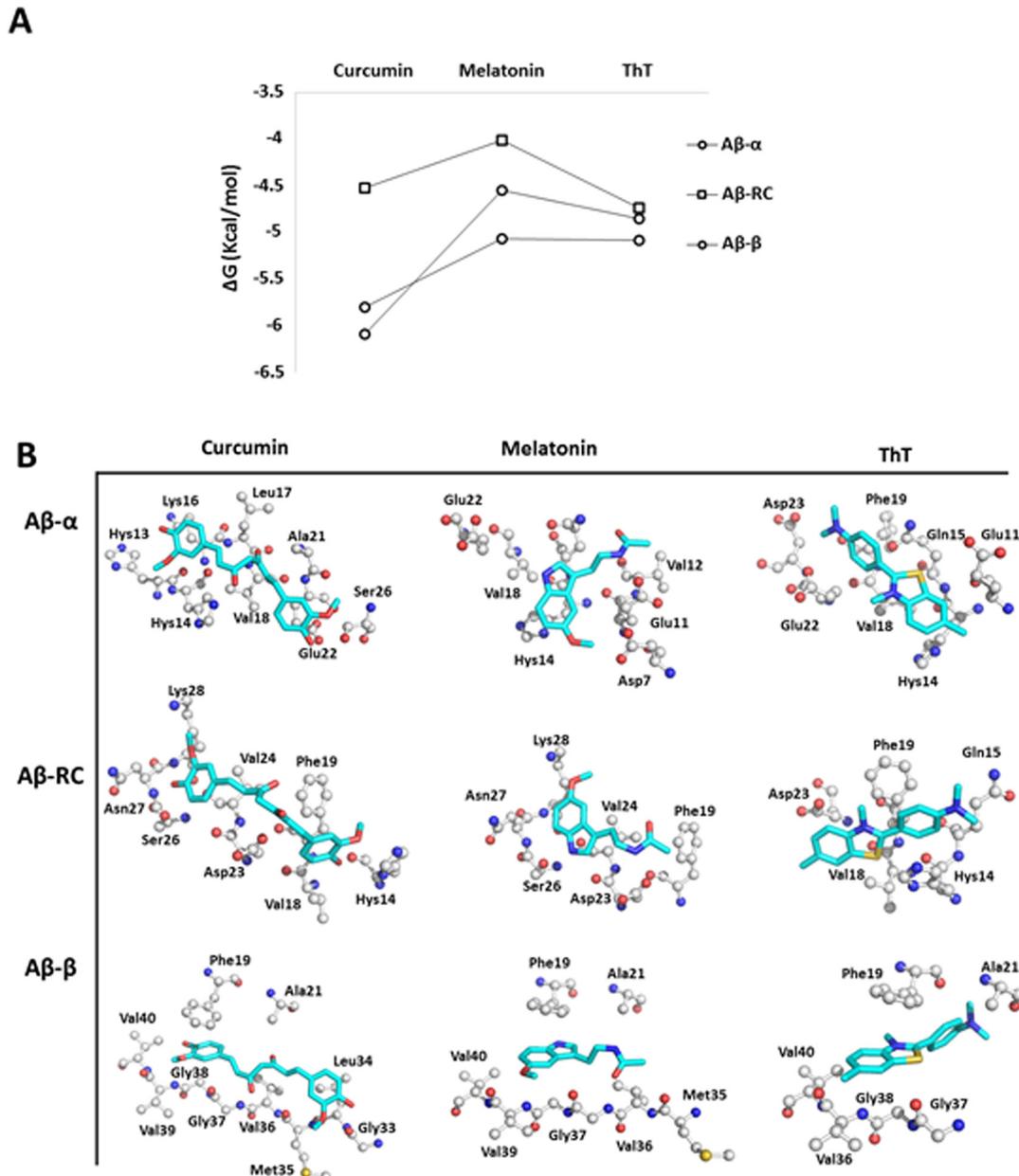
Fig 8. Docking results between curcumin, melatonin and ThT with several Aβ$_{1-42}$ conformers. The methodology to obtain the complex is the same as mentioned above for the docking studies with the selected compounds. ΔG values were obtained through docking studies of the ligands with **Aβ-α** (circles), **Aβ-RC** (rhombuses) and **Aβ-β** (squares) (A). The binding modes of curcumin, melatonin and ThT on **Aβ-α**, **Aβ-RC**, and **Aβ-β** (B).

doi:10.1371/journal.pone.0130263.g008

establishment of electrostatic interactions with Glu22 and Asp23, π–π interactions with Phe19 and Phe20, and the presence of aliphatic substituents in the aromatic rings to establish hydrophobic interactions with the methylene side chain of Lys16. These findings allow for the identification of potential pharmacophores to inhibit Aβ$_{1-42}$ oligomerization and to prevent the formation of oligomeric species.

Acknowledgments

Author Contributions

Conceived and designed the experiments: JCB MCRH MHR. Performed the experiments: MHR JVMM MINV CGBC. Analyzed the data: MCRH JCB MHR CGBC. Contributed reagents/materials/analysis tools: JCB MCRH MINV RMR AARA. Wrote the paper: MHR MCRH JCB MINV.

References

1. Glenner GG, Wong CW, Quaranta V, Eanes ED. The amyloid deposits in Alzheimer's disease: their nature and pathogenesis. Appl Pathol. 1984; 2: 357–369. PMID: 6242724

2. Selkoe DJ. The molecular pathology of Alzheimer's disease. Neuron. 1991; 6: 487–498. PMID: 1673054

3. Hardy J, Selkoe DJ. The amyloid hypothesis of Alzheimer's disease: progress and problems on the road to therapeutics. Science. 2002; 297: 353–356. PMID: 12130773

4. De Strooper B, Vassar R, Golde T. The secretases: enzymes with therapeutic potential in Alzheimer disease. Nat Rev Neurol. 2010; 6: 99–107. doi: 10.1038/nrneurol.2009.218 PMID: 20139999

5. Sciarretta KL, Gordon DJ, Petkova AT, Tycko R, Meredith SC. Abeta40-Lactam (D23/K28) models a conformation highly favorable for nucleation of amyloid. Biochemistry. 2005; 44: 6003–6014. PMID: 15835889

6. Kirkitadze MD, Condron MM, Teplow DB. Identification and characterization of key kinetic intermediates in amyloid beta-protein fibrillogenesis. J Mol Biol. 2001; 312: 1103–1119. PMID: 11580253

7. Walsh DM, Klyubin I, Fadeeva JV, Rowan MJ, Selkoe DJ. Amyloid-beta oligomers: their production, toxicity and therapeutic inhibition. Biochem Soc Trans. 2002; 30: 552–557. PMID: 12196135

8. Lambert MP, Barlow AK, Chromy BA, Edwards C, Freed R, Liosatos M, et al. Diffusible, nonfibrillar ligands derived from Abeta1-42 are potent central nervous system neurotoxins. Proc Natl Acad Sci USA. 1998; 95: 6448–6453. PMID: 9600986

9. Walsh DM, Klyubin I, Fadeeva JV, Cullen WK, Anwyl R, Wolfe MS, et al. Naturally secreted oligomers of amyloid beta protein potently inhibit hippocampal long-term potentiation in vivo. Nature. 2002; 416: 535–539. PMID: 11932745

10. LeVine H III. Small molecule inhibitors of Abeta assembly. Amyloid. 2007; 14: 185–197. PMID: 17701466

11. Salomon AR, Friedland RP, Zagorski MG. Nicotine inhibits amyloid formation by the beta-peptide. Biochemistry. 1996; 35: 13568–13578. PMID: 8885836

12. Pappolla M, Bozner P, Soto C, Shao H, Robakis NK, Zagorski M, et al. Inhibition of Alzheimer beta-fibrillogenesis by melatonin. J Biol Chem. 1998; 273: 7185–7188. PMID: 9516407

13. Mason JM, Kokkoni N, Stott K, Doig AJ. Design strategies for anti-amyloid agents. Curr Opin Struct Biol. 2003; 13: 526–532. PMID: 12948784

14. Orlando RA, Gonzales AM, Royer RE, Deck LM, Vander Ja DL. A chemical analog of curcumin as an improved inhibitor of amyloid Abeta oligomerization. PLoS One. 2012; 7, e31869. doi: 10.1371/journal.pone.0031869 PMID: 22442659

15. Shaw JE, Chio J, Dasgupta S, Lai AY, Mo GC, Pang F, et al. Aβ (1–42) Assembly in the presence of scyllo-inositol derivatives: identification of an oxime linkage as important for the development of assembly inhibitors. ACS Chem Neurosci. 2012; 3: 167–177. doi: 10.1021/cn2000926 PMID: 22860186

16. Merlini G, Ascari E, Amboldi N, Bellotti V, Arbustini E, Perfetti V, et al. Interaction of the anthracycline 4'-iodo-4-deoxydoxorubicin with amyloid fibrils: Inhibition of amyloidogenesis. Proc Natl Acad Sci USA. 1995; 92: 2959–2963. PMID: 7708755

17. Esteras-Chopo A, Morra G, Moroni E, Serrano L, Lopez de la Paz M, Colombo G. A molecular dynamics study of the interaction of D-peptide amyloid inhibitors with their target sequence reveals a potential inhibitory pharmacophore conformation. J Mol Biol. 2008; 383: 266–280. doi: 10.1016/j.jmb.2008.07.076 PMID: 18703072

18. Cohen FE, Kelly JW. Therapeutic approaches to protein-misfolding diseases. Nature. 2003; 426: 905–909. PMID: 14685252

19. Landau M, Sawaya MR, Faull KF, Laganowsky A, Jiang L, Sievers SA, et al. Towards a pharmacophore for amyloid. PLoS. Biol. 2011; 9: e1001080. doi: 10.1371/journal.pbio.1001080 PMID: 21695112

20. Nerelius C, Sandegren A, Sargsyan H, Raunak R, Leijonmarck H, Chatterjee U, et al. α-Helix targeting reduces amyloid-β peptide toxicity. Proc Natl Acad Sci USA. 2009; 106: 9191–9196. doi: 10.1073/pnas.0810364106 PMID: 19458258

21. Ito M, Johansson J, Strömberg R, Nilsson L. Unfolding of the amyloid b-peptide central helix: mechanistic insights from molecular dynamics simulations. PLoS One. 2011; 3: 1–13.

22. Bansode SB, Jana AK, Batkulwar KB, Warkad SD, Joshi RS, Sengupta N, et al. Molecular investigations of protriptyline as a multi-target directed ligand in Alzheimer's disease. PLoS One. 2014; 9: e105196. doi: 10.1371/journal.pone.0105196 PMID: 25141174

23. Cui L, Zhang Y, Cao H, Wang Y, Teng T, Ma G, et al. Ferulic acid inhibits the transition of amyloid-β42 monomers to oligomers but accelerates the transition from oligomers to fibrils. J Alzheimers Dis. 2013; 37: 19–28. doi: 10.3233/JAD-130164 PMID: 23727899

24. Aloisi A, Barca A, Romano A, Guerrieri S, Storelli C, Rinaldi R, et al. Anti-aggregating effect of the naturally occurring dipeptide carnosine on aβ1–42 fibril formation. PLoS One. 2013; 8: e68159. doi: 10.1371/journal.pone.0068159 PMID: 23844165

25. Singh SK, Gaur R, Kumar A, Fatima R, Mishra L, Srikrishna S. The flavonoid derivative 2-(4' Benzyloxyphenyl)-3-hydroxy-chromen-4-one protects against Aβ42-induced neurodegeneration in transgenic Drosophila: insights from in silico and in vivo studies. Neurotox Res. 2014; 26:331–350 doi: 10.1007/s12640-014-9466-z PMID: 24706035

26. Hernández-Rodríguez M, Correa-Basurto J, Benitez-Cardoza CG, Resendiz-Albor AA, Rosales-Hernández MC. In silico and in vitro studies to elucidate the role of Cu2+ and galantamine as the limiting step in the amyloid beta (1–42) fibrillation process. Protein Sci. 2013; 22: 1320–1335. doi: 10.1002/pro.2319 PMID: 23904252

27. Frishman D, Argos P. Knowledge-Based Protein Secondary Structure Assignment. Proteins. 1995; 23: 566–579. PMID: 8749853

28. Morris GM, Goodsell DS, Halliday RS, Huey R, Hart WE, Belew RK, et al. Automated docking using a Lamarckian genetic algorithm and empirical binding free energy function. J Computat Chem.1998; 19: 1639–1662.

29. G Dewar MJ, Zoebish EG, Healey EF, Stewart JP. Development and use of quantum mechanical molecular models. 76. AM1: a new general purpose quantum mechanical molecular model. J. Am. Chem. Soc. 1985; 107: 3902.

30. Seeliger D, de Groot BL. Ligand docking and binding site analysis with PyMOL and Autodock/Vina. J Comput Aided Mol Des. 2010; 24: 417–422. doi: 10.1007/s10822-010-9352-6 PMID: 20401516

31. Levine H. Thioflavine T interaction with synthetic Alzheimer's disease beta-amyloid peptides: detection of amyloid aggregation in solution. Protein Sci. 1993; 2: 404–410. PMID: 8453378

32. Sreerama N, Woody RW. A self-consistent method for the analysis of protein secondary structure from circular dichroism. Anal Biochem. 1993; 209: 32–44. PMID: 8465960

33. Perez-Iratxeta C, Andrade-Navarro MA. K2D2: Estimation of protein secondary structure from circular dichroism spectra. BMC Struct Biol. 2008; 8: 25. doi: 10.1186/1472-6807-8-25 PMID: 18477405

34. Fukui K. Role of frontier orbitals in chemical reactions. Science. 1982; 218: 747–754. PMID: 17771019

35. Politzer P, Laurence PR, Jayasuriya K. Molecular Electrostatic Potentials: An Effective Tool for the Elucidation of Biochemical Phenomena. Environ Health Perspect. 1985; 61: 191–202. PMID: 2866089

36. Hehre WJ, Shusterman AJ, Nelson JE. The Molecular Modeling Workbook for Organic Chemistry, Wavefunction, Inc. 1998. 18401 Von Karman Ave., Suite 370 Irvine, CA 92612, pp 29–31 and 50–51.

37. Hunter CA. Quantifying intermolecular interactions: guidelines for the molecular recognition toolbox Angew. Chem Int. 2004. Ed. 43, 5310–5324.

38. Fezoui Y, Teplow DB. Kinetic studies of amyloid beta-protein fibril assembly. Differential effects of alpha-helix stabilization. J Biol Chem. 2002; 277: 36948–36954. PMID: 12149256

39. Wheeler SE, Houk KN. Through-space effects of substituents dominate molecular electrostatic potentials of substituted arenes. J Chem Theor Comput. 2009; 5: 2301–2312.

40. Chebaro Y, Jiang P, Zang T, Mu Y, Nguyen PH, Mousseau N, et al. Structures of Aβ17–42 trimers in isolation and with five small-molecule drugs using a hierarchical computational procedure. J Phys Chem B. 2012; 116: 8412–8422. doi: 10.1021/jp2118778 PMID: 22283547

41. Xie Q, Wang H, Xia Z, Lu M, Zhan W, Wang X, et al. Bis-(-)-nor-meptazinols as novel nanomolar cholinesterase inhibitors with high inhibitory potency on amyloid-beta aggregation. J Med Chem. 2008; 51: 2027–2036. doi: 10.1021/jm070154q PMID: 18333606

42. Cardoso FL, Brites D, Brito MA. Looking at the blood-brain barrier: molecular anatomy and possible investigation approaches. Brain Res Rev. 2010; 64: 328–363. doi: 10.1016/j.brainresrev.2010.05.003 PMID: 20685221

43. Doig AJ, Derreumaux P. Inhibition of protein aggregation and amyloid formation by small molecules. Curr Opin Struct Biol. 2015; 30: 50–56. doi: 10.1016/j.sbi.2014.12.004 PMID: 25559306

44. Nasica-Labouze J, Nguyen PH, Sterpone F, Berthoumieu O, Buchete NV, Coté S, et al. Amyloid β Protein and Alzheimer's Disease: When Computer Simulations Complement Experimental Studies. Chem Rev. 2015; 115: 3518–3563 doi: 10.1021/cr500638n PMID: 25789869

45. Tarus B, Nguyen PH, Berthoumieu O, Faller P, Doig AJ, Derreumaux P. Molecular structure of the NQTrp inhibitor with the Alzheimer Aβ1–28 monomer. Eur J Med Chem. 2015; 91: 43–50. doi: 10.1016/j.ejmech.2014.07.002 PMID: 25011560

46. Novick PA, Lopes DH, Branson KM, Esteras-Chopo A, Graef IA, Bitan G, et al. Design of β-amyloid aggregation inhibitors from a predicted structural motif. J Med Chem. 2012; 55: 3002–3010. doi: 10.1021/jm201332p PMID: 22420626

47. Matsubara E, Takamura A, Okamoto Y, Oono H, Nakata T, Wakasaya Y, et al. Disease modifying therapies for Alzheimer's disease targeting a β oligomers: implications for therapeutic mechanisms. Biomed Res Int. 2013; 2013: 984041. doi: 10.1155/2013/984041 PMID: 24063020

48. Li J, Yang JY, Yao XC, Xue X, Zhang QC, Wang XX, et al. Oligomeric Aβ-induced microglial activation is possibly mediated by NADPH oxidase. Neurochem Res. 2013; 38: 443–452. doi: 10.1007/s11064-012-0939-2 PMID: 23229789

49. Lue LF, Kuo YM, Roher AE, Brachova L, Shen Y, Sue L, et al. Soluble amyloid beta peptide concentration as a predictor of synaptic change in Alzheimer's disease. Am J Pathol. 1999; 155: 853–862. PMID: 10487842

50. Dahlgren KN, Manelli AM, Stine WB Jr, Baker LK, Krafft GA, LaDu MJ. Oligomeric and fibrillar species of amyloid-beta peptides differentially affect neuronal viability. J Biol Chem. 2002; 277: 32046–32053. PMID: 12058030

51. Selkoe DJ, Schenk D. Alzheimer's disease: molecular understanding predicts amyloid-based therapeutics. Annu Rev Pharmacol Toxicol. 2003; 43: 545–584. PMID: 12415125

52. Chen WT, Liao YH, Yu HM, Cheng IH, Chen YR. Distinct effects of Zn2+, Cu2+, Fe3+, and Al3+ on amyloid-beta stability, oligomerization, and aggregation: amyloid-beta destabilization promotes annular protofibril formation. J Biol Chem. 2011; 286: 9646–9656. doi: 10.1074/jbc.M110.177246 PMID: 21216965

53. Zhang T, Xu W, Mu Y, Derreumaux P. Atomic and dynamic insights into the beneficial effect of the 1,4-naphthoquinon-2-yl-L-tryptophan inhibitor on Alzheimer's Aβ1–42 dimer in terms of aggregation and toxicity. ACS Chem Neurosci. 2014; 5: 148–159. doi: 10.1021/cn400197x PMID: 24246047

54. Nguyen P, Derreumaux P. Understanding amyloid fibril nucleation and aβ oligomer/drug interactions from computer simulations. Acc Chem Res. 2014; 47:603–611. doi: 10.1021/ar4002075 PMID: 24368046

55. Yadav A, Sonker M. Perspectives in designing anti aggregation agents as Alzheimer disease drugs. Eur J Med Chem. 2009; 44: 3866–3873. doi: 10.1016/j.ejmech.2009.04.013 PMID: 19497645

56. Pohl G, Plumley JA, Dannenberg JJ. The interactions of phenylalanines in β-sheet-like structures from molecular orbital calculations using density functional theory (DFT), MP2, and CCSD(T) methods. J Chem Phys. 2013; 138: 245102. doi: 10.1063/1.4811712 PMID: 23822281

57. Chadwick W, Mitchell N, Caroll J, Zhou Y, Park SS, Wang L, et al. Amitriptyline-mediated cognitive enhancement in aged 3×Tg Alzheimer's disease mice is associated with neurogenesis and neurotrophic activity. PLoS One. 2011; 6: e21660. doi: 10.1371/journal.pone.0021660 PMID: 21738757

58. Matharu B, Gibson G, Parsons R, Huckerby TN, Moore SA, Cooper LJ, et al. Galantamine inhibits b-amyloid aggregation and cytotoxicity. J Neurol Sci. 2009; 280: 49–58. doi: 10.1016/j.jns.2009.01.024 PMID: 19249060